Study on Photoluminescence and Thermoluminescence of $Y_{2-x}Sm_xMgTiO_6$ Phosphors*

Hao Liu,[1] Lu-Yan Wang,[1] Zheng-Ye Xiong,[1,†] and Jing-Yuan Guo[1,‡]

[1]*School of Electronic and Information Engineering, Guangdong Ocean University Zhan'jiang 524088 China*

In recent years, double perovskite matrix materials have gained significant attention due to their flexible structure, ease of doping and excellent thermal stability. While studies related to photoluminescence in rare-earth-doped double perovskite matrix materials are common, research specifically focused on thermoluminescence remains relatively scarce. In this study, a series of $Y_{2-x}Sm_xMgTiO_6$ ($0 \le x \le 0.1$) samples were synthesized using high-temperature solid-state methods. XRD analysis revealed that the crystal structure of the samples belongs to the monoclinic system (space group $P2_1/n$), with Sm^{3+} ions substituting for Y^{3+} ions in Y_2MgTiO_6. The PL results indicated that the optimal doping concentration was $Y_{1.95}Sm_{0.05}MgTiO_6$, which exhibited emission peaks at 568 nm, 605 nm, 652 nm, and 715 nm under blue light excitation at 409 nm. TL measurements for different doping concentrations showed that $Y_{1.98}Sm_{0.02}MgTiO_6$ phosphors exhibited the strongest TL signal. The TL peaks observed at 530 K and 610 K corresponded to defects in the matrix and Sm^{3+} dopants, respectively. The T_m-T_{stop} analysis revealed that the TL curve of $Y_{1.98}Sm_{0.02}MgTiO_6$ phosphors was a superposition of seven peaks. Computerized glow curve deconvolution (CGCD) was performed on the TL of the sample according to the results of three-dimensional thermoluminescence spectra (3D-TL) and T_m-T_{stop}, the trap depths in the sample were estimated to range from 0.69 eV to 1.49 eV. Additionally, the lifetimes of each overlapping peak were calculated using fitting parameters. Furthermore, the dose response test showed that the saturation dose of the sample was higher, which was 9956 Gy. Therefore, this material can serve as a thermoluminescence dosimeter for high-dose measurements. The saturation dose for the lowest-temperature overlapping peak was found to be 102 Gy, which correlates with its specific energy level lifetime, while other overlapping peaks also exhibited favorable linear relationships.

Keywords: Y_2MgTiO_6; Thermoluminescence; T_m-T_{stop}; Computerized Glow Curve Deconvolution; Dose Response

I. INTRODUCTION

Studies have shown that the optical and dosimetric properties of oxide matrix materials doped with rare earth ions may be improved[1–5]. Among the oxide matrix materials, double perovskites have attracted much attention due to their excellent chemical structure and good stability[6]. AA'BB'O_6-type double perovskites can be obtained by partially substituting A or B sites of ABO_3-type simple perovskites with different A' or B' ions. As a new type of matrix material, the structure and luminescence properties of double perovskites have been extensively studied. For example, La_2MgTiO_6[7], Gd_2ZnTiO_6[8], La_2MTiO_6(M=Co,Ni) [9]have good thermal stability and superior luminescence properties, which can be used as candidate materials in the field of lighting. However, their thermoluminescence properties have rarely been studied. Y_2MgTiO_6 matrix material has become a research hotspot in recent years due to its physicochemical stability, easy preparation, and wide availability of raw materials[10].

Thermoluminescent materials contain a certain concentration of luminescent centers and traps. Under high-energy radiation excitation, free electrons and holes are generated in the crystal, and some of them are captured by the traps. When the crystal is heated, the captured electrons (or holes) are thermally excited to become quasi-free carriers, and thermoluminescence is produced when the quasi-free carriers recombine with the luminescent centers[11, 12]. The analysis of the thermoluminescence glow curve can estimate the types and activation energies of the traps[13–16]. Most of the current researches use the Computerized Glow Curve Deconvolution (CGCD) method for analysis. If the internal information of the system is not known, this method will lack physical meaning. If the luminescence characteristics of the thermoluminescent material can be further understood, the results can be more accurate and reliable. Many thermoluminescent materials have good linearity of dose response, easy fabrication, and low cost[17–19], and can be used for ionizing radiation dose detection. For example, LiF:Mg,Cu,P[20], $Li_2B_4O_7$:Mn[21] can be used for personal dose detection; BeO[22], $CaSO_4$:Dy[23], CaF_2:Dy [24]can be used for environmental dose detection; Al_2O_3:C[25], MgB_4O_7:Dy[26] can be applied to medical dose detection. In addition to the standard thermoluminescence dosimeters, there are other materials that may be used for dose detection, such as $SrGd_2O_4$:Sm^{3+}, $SrDy_2O_4$:Eu^{3+}, $BaSi_2O_5$:Dy^{3+}, (Sr,Ba)AlO_4:Eu^{2+}/Dy^{3+}, $CaWO_4$:Pr^{3+}, $LaGa_4O(BO_3)_3$ and (Ba,Sr)TiO_3:Pr^{3+} [27–32]. The sensitivity of general thermoluminescence dosimeters is high, but the linear upper limit of dose response is generally not very high (about 200 Gy). In some special occasions (such as irradiation preservation), it is often necessary to accurately measure the irradiation dose of kGy level[33, 34]. Therefore, the study of thermoluminescent

* Zhanjiang Science and Technology Plan Project (2022A05022); Science and Technology Development Special Project of Zhanjiang (2023A21616); Research Project of Guangdong Ocean University (060302112102)

† Corresponding author, name: Zheng-Ye Xiong. address: Guangdong Ocean University, zhanjiang, guangdong. e-mail: xiongzhengye@139.com. Tel: 15913501619.

‡ Corresponding author, name: Jing-Yuan Guo. address: Guangdong Ocean University, zhanjiang, guangdong. e-mail: gjy3344@126.com. Tel: 13434332773.

materials with stable performance and wide range of dose response linearity can expand the application field of thermoluminescence technology.

Sm^{3+} single-doped Y_2MgTiO_6 phosphor was prepared by high-temperature solid-state method, and its X-ray diffraction spectrum (XRD), photoluminescence spectrum (PL) and thermoluminescence (TL) were measured. The thermoluminescence internal mechanism of the sample with the best TL yield and the possibility of being used as a thermoluminescence dosimeter material and high dose detection were studied by three-dimensional thermoluminescence spectroscopy (3D-TL) , T_m-T_{stop} analysis, CGCD method and dose response.

II. EXPERIMENT

A. Sample preparation

$Y_{2-x}Sm_xMgTiO_6$ (x=0, 0.001, 0.002, 0.005, 0.01, 0.02, 0.05, 0.1 and 0.2) series phosphors were synthesized by high-temperature solid-state method. A certain amount of Y_2O_3 (99.99%), MgO (99.99%), TiO_2 (99.99%), Sm_2O_3 (99.99%) were weighed according to the stoichiometric ratio and placed in an agate mortar. They were fully ground for 0.5 h until uniformly mixed. The uniformly ground powder was placed in a corundum crucible and placed in a muffle furnace. It was pre-sintered at 800 °C for 3 h in air atmosphere to prepare for the solid phase of the material, and heated to 1300 °C at a faster heating rate (7 °C/s) and then calcined at 1300 °C for 9 h. The block-shaped sintered samples were obtained, and the block-shaped samples were crushed and ground with an agate mortar to obtain phosphor powder.

B. Testing method

The XRD of different samples was measured by Rigaku Ultima IV X-ray diffractometer. Cu-Kα radiation source was used for measurement, scanning range was 10°-80°, and scanning rate was 5 °/min. The PL of the samples was measured by HITACHI F-7000 fluorescence spectrometer. The excitation light source was Xe lamp, and the spectral resolution was 0.2 nm. The TL of the samples was measured by Risø TL/OSL-15-B/C thermoluminescence/optically stimulated luminescence measurement instrument. The irradiation source was $^{90}Sr\beta$ radiation source equipped with the instrument, the dose rate was about 0.1 Gy/s, the radioactivity of $^{90}Sr\beta$ radiation source was 1.4 GBq, the distance between $^{90}Sr\beta$ radiation source and the sample was 5 mm, the distance between the detector and the sample was 55 mm, and the heating rate was 5 K/s during measurement. The three-dimensional thermoluminescence spectroscopy of the samples was measured by LTTL3DS thermoluminescence spectrometer (Guangzhou Ruidi Technology Co., Ltd.). The irradiation source was X-ray tube, the working voltage of X-ray tube was 50 kV, the current was 150 μA, the dose rate was about 0.1 Gy/s, the heating rate was 5 K/s during measurement, the heating range was 300-750 K, the spectral range was 300-1000 nm, and the spectral resolution was 1 nm.

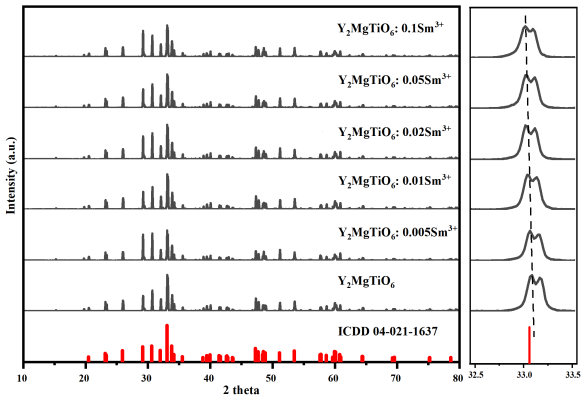

Fig. 1. XRD Spectra of $Y_{2-x}Sm_xMgTiO_6$ (x=0, 0.005, 0.01, 0.02, 0.05 and 0.1) Samples

III. RESULTS AND DISCUSSION

A. XRD analysis

The XRD patterns of $Y_{2-x}Sm_xMgTiO_6$ (x=0, 0.005, 0.01, 0.02, 0.05 and 0.1) series samples are shown in Fig. 1. There is no information of Y_2MgTiO_6 in the inorganic crystal information database. Shannon[35] used the Rietveld method to analyze the data, and the results proved that Dy_2MgTiO_6 and Y_2MgTiO_6 have very similar structures. Therefore, the standard card of Dy_2MgTiO_6 (ICDD 04-021-1637) was used as a reference. As can be seen from the figure, the number and position of the X-ray diffraction peaks of different samples are basically consistent with the standard card, and the diffraction angle (33°) belonging to the characteristic site of Y^{3+} shifts to a small angle[36, 37]. According to the Bragg equation[38, 39], the diffraction angle shifts to a small angle indicates that the lattice spacing increases. The ionic radii of each element in the lattice system are rY^{3+}=0.1019 nm, rMg^{2+}=0.0720 nm, rTi^{4+}=0.0605 nm[40], and the ionic radius of Sm^{3+} is rSm^{3+}=0.1132 nm. The shift of the diffraction angle of the characteristic site of Y^{3+} to a small angle can prove that Sm^{3+} with a larger ionic radius successfully enters the lattice to replace Y^{3+} with a smaller ionic radius, and does not change the lattice structure and charge configuration. The sample is still monoclinic $P2_1\backslash n$[37].

Fig.2 is the morphology and lattice fringes of Y_2MgTiO_6 matrix and Y_2MgTiO_6: Sm. It can be seen in the figure that the morphology of the phosphor is irregular, the larger size particles are 2 μm and the smaller size particles are 400 nm, and the lattice fringes become more dense after doping Sm, which means that the crystal plane spacing decreases, which proves that Sm with larger ion radius successfully enters the matrix lattice. Combined with XRD results, it can be seen

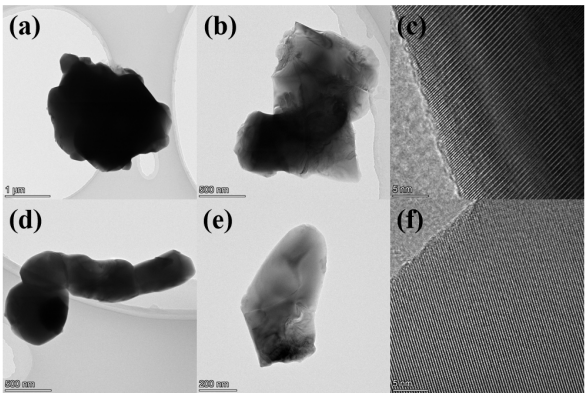

Fig. 2. XRD Spectra of $Y_{2-x}Sm_xMgTiO_6$ (x=0, 0.005, 0.01, 0.02, 0.05 and 0.1) Samples

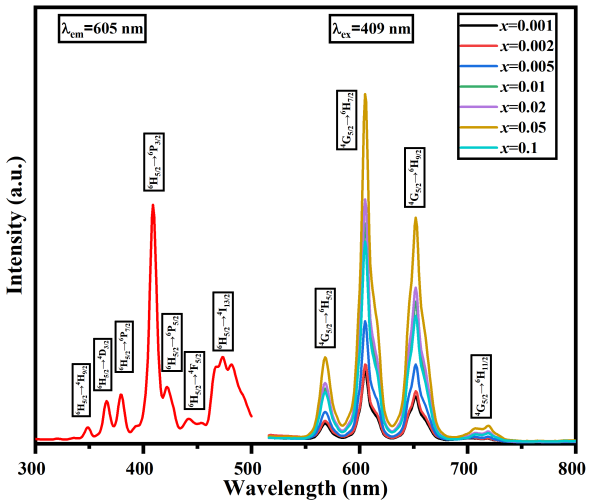

Fig. 3. Photoluminescence spectra of $Y_{2-x}Sm_xMgTiO_6$ (x=0.001, 0.002, 0.005, 0.01, 0.02, 0.05 and 0.1) samples

that the phosphor was successfully prepared under this experimental conditions.

B. Photoluminescence analysis

Fig. 3 shows the PL of $Y_{2-x}Sm_xMgTiO_6$ (x=0.001, 0.002, 0.005, 0.01, 0.02, 0.05 and 0.1) series phosphors. When the monitoring wavelength is 605 nm, the excitation spectrum can be extended from 340 nm to 500 nm. The strongest absorption peak is at 409 nm, which belongs to the characteristic transition of Sm^{3+} $^6H_{5/2}\rightarrow{}^6P_{3/2}$. The absorption peaks at 349 nm, 366 nm, 379 nm, 422 nm, 443 nm, and 474 nm correspond to the characteristic transitions of Sm^{3+} $^6H_{5/2}\rightarrow{}^4H_{9/2}$, $^4D_{3/2}$, $^6P_{7/2}$, $^6P_{5/2}$, $^4F_{5/2}$, $^4I_{13/2}$, respectively[41]. When excited by 409 nm purple light, there are four obvious emission peaks, located at 568 nm, 605 nm, 652 nm and 715 nm, corresponding to the characteristic transitions of Sm^{3+} $^4G_{5/2}\rightarrow{}^6H_{5/2}$, $^6H_{7/2}$, $^6H_{9/2}$, $^6H_{11/2}$, respectively[42, 43]. With the increase of Sm^{3+} doping concentration, the position and shape of the emission peaks do not change, and the emission intensity first increases and then decreases. When the Sm^{3+} doping concentration is x=0.05, the photoluminescence emission intensity is the largest, and obvious concentration quenching phenomenon occurs in the system with the continuous increase of doping concentration.

C. Doping concentration optimization

In order to determine the phosphor with the best TL yield, the thermoluminescence peak was optimized by changing the doping concentration of Sm^{3+}. Samples with different doping concentrations were weighed 30 mg each, and then TL test was performed. The test steps are as follows: 1) preheat the sample to 773 K and hold for 10 s; 2) cool to room temperature; 3)irradiate with $^{90}Sr\beta$ radiation source for 100 Gy; 4) measure TL (heating rate is 5 K/s). The measurement results are shown in Fig. 4. As can be seen from the figure, with the increase of Sm^{3+} doping concentration, the thermoluminescence integral intensity gradually increases, and reaches the strongest when the Sm^{3+} doping concentration is x=0.02, this sample was analyzed in subsequent experiments. With the introduction of more Sm^{3+}, concentration quenching effect occurs, and the thermoluminescence integral intensity decreases. It can be seen from the figure that the Y_2MgTiO_6 matrix has a weak thermoluminescence peak, and the thermoluminescence range is between 460 K and 630 K. After introducing Sm^{3+}, the thermoluminescence peak of the phosphor is obviously extended to the high temperature zone, and there is also obvious thermoluminescence at 675 K. In addition, the shape of the thermoluminescence curve changes with the change of Sm^{3+} doping concentration. As can be seen from the inset in Fig. 3, when the Sm^{3+} doping concentration is x<0.02, the thermoluminescence peak value around 610 K is stronger, significantly larger than the peak intensity around 530 K. When the Sm^{3+} doping concentration is x>0.02, the thermoluminescence peak around 530 K is larger than the peak intensity around 610 K. When the Sm^{3+} doping concentration is x=0.02, a wonderful balance state is reached. When the concentration quenching occurs, the decrease rate of the peak intensity around 610 K is obviously faster than that of the peak intensity at 530 K.

To explain the reasons for these situations and to further understand the internal mechanism of thermoluminescence of $Y_{2-x}Sm_xMgTiO_6$ series phosphors, the three-dimensional thermoluminescence spectra of four standard samples irradiated by X-rays for 100 Gy were made, as shown in Fig. 5. Fig. 5a shows that the thermoluminescence range of Y_2MgTiO_6 matrix is between 480 K and 640 K, the peak temperature is at 530 K and 600 K, which is basically consistent with the curve in Fig. 4, and the characteristic emission band of Y_2MgTiO_6 matrix thermoluminescence is around 698 nm. Fig. 5b is the three-dimensional thermoluminescence spectrum when $0.01Sm^{3+}$ is introduced. It can be seen that the

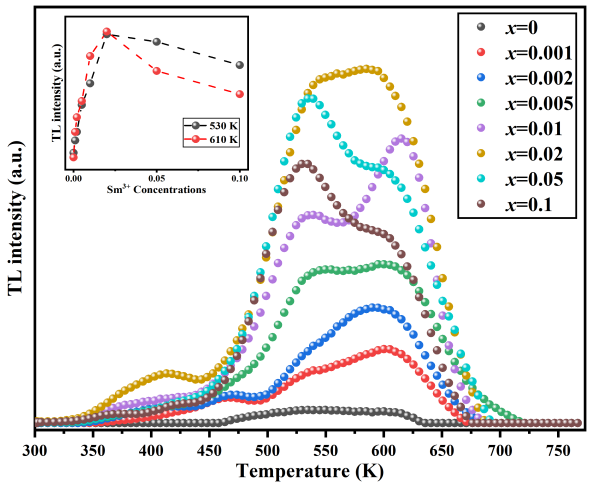

Fig. 4. The thermoluminescence spectra of $Y_{2-x}Sm_xMgTiO_6$(x=0, 0.001, 0.002, 0.005, 0.01, 0.02, 0.05 and 0.1) samples by irradiate with $^{90}Sr\beta$ radiation source for 100 Gy. The variation trend of thermoluminescence intensity with Sm^{3+} doping concentration at 530 K and 610 K is illustrated.

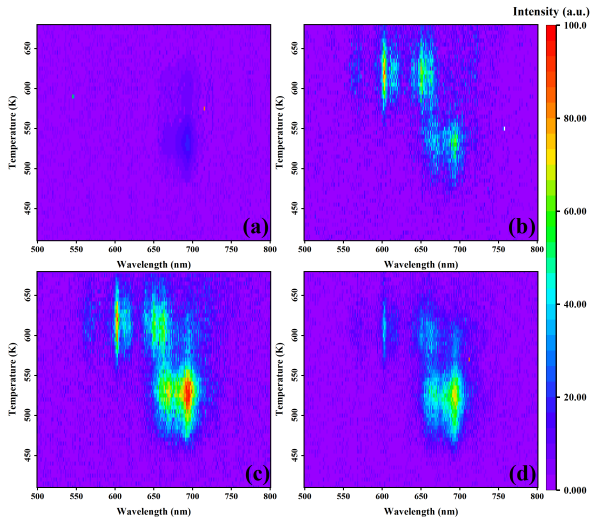

Fig. 5. The thermoluminescence spectra of Y_2MgTiO_6 (a),$Y_{1.99}Sm_{0.01}MgTiO_6$ (b),$Y_{1.98}Sm_{0.02}MgTiO_6$ (c) and $Y_{1.9}Sm_{0.1}MgTiO_6$ (d) samples by irradiate with X-Ray source for 100 Gy.

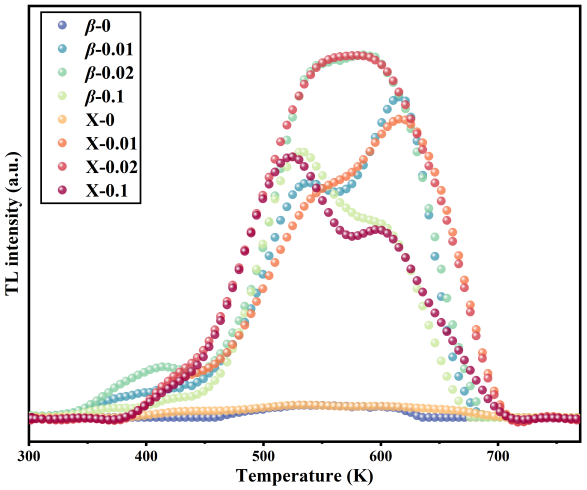

Fig. 6. Thermoluminescence spectra of $Y_{2-x}Sm_xMgTiO_6$ phosphors irradiated by X-ray and -particles at 100 Gy.

introduction of Sm^{3+} enhances the thermoluminescence intensity of Y_2MgTiO_6 matrix, and does not change the peak temperature and emission band position of the matrix thermoluminescence, and a new thermoluminescence peak appears around 610 K, the emission band is around 570 nm, 600 nm, 650 nm, which is basically consistent with the characteristic emission shown by Sm^{3+} in PL, from which it can be inferred that the thermoluminescence peak here is caused by Sm^{3+}, the thermoluminescence intensity caused by Sm^{3+} is obviously larger than that of the matrix, that is, the peak intensity around 610 K is obviously larger than that of 530 K, which is also consistent with the curve in Fig. 4. The three-dimensional thermoluminescence spectrum of Sm^{3+} doping concentration x=0.02 is shown in Fig. 5c. It can be found that with the continuous increase of Sm^{3+} doping concentration, not only the thermoluminescence intensity of Sm^{3+} is enhanced, but also the thermoluminescence intensity of the matrix is enhanced. At this time, the thermoluminescence peak (610 K) intensity caused by Sm^{3+} is basically consistent with the thermoluminescence peak (530 K) intensity caused by the matrix, so a balance state is reached in the thermoluminescence spectrum. Then, with the continuous increase of Sm^{3+} doping concentration, the thermoluminescence intensity caused by Sm^{3+} decreases significantly, and the thermoluminescence peak caused by the matrix also decreases, but the decrease is much smaller than that of Sm^{3+}, which indicates that the thermoluminescence emission of Sm^{3+} is greatly affected by the concentration quenching effect, but the concentration quenching effect has little effect on the matrix, which also explains the reason why the thermoluminescence peak intensity of 530 K is larger than that of 610 K after excessive introduction of Sm^{3+}.

In order to determine the energy dependence under X-ray and β -particles irradiation, the thermoluminescence spectra of four samples under X-ray irradiation were measured by Risø instrument, and compared with the thermoluminescence spectra under β -particles irradiation. The results are shown in Fig.6. It can be found that the thermoluminescence spectra under X-ray irradiation and β -particles irradiation are basically the same, and there is a slight difference in the low temperature region.

D. T_m-T_{stop} method

To confirm the number of overlapping peaks and their peak temperatures in the thermoluminescence (TL) spectrum of the $Y_{1.98}Sm_{0.02}MgTiO_6$ sample, enabling fitting using the

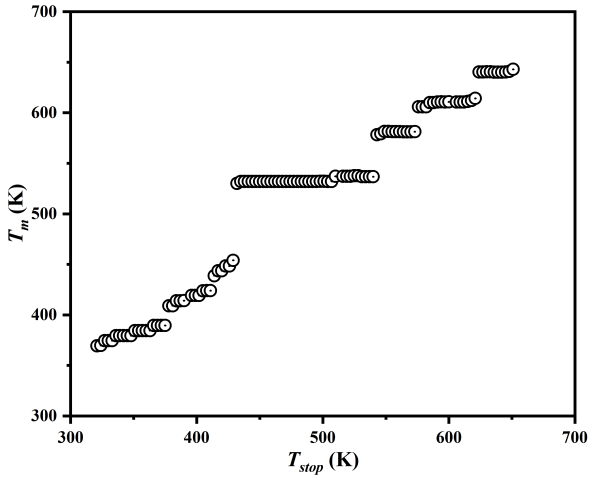

Fig. 7. T_m-T_{stop} diagram of $Y_{1.98}Sm_{0.02}MgTiO_6$ sample

CGCD method and further exploring the thermal luminescence mechanism and kinetic parameters of the sample. Peak separation experiments were performed using the T_m-T_{stop} method. The test steps of the T_m-T_{stop} method are as follows:

1. Preheat the sample to 773 K and hold for 10 seconds.
2. Cool the sample to room temperature.
3. Irradiate the sample with a $^{90}Sr\beta$ radiation source at a dose of 100 Gy.
4. Heat the sample to a high enough temperature (T_{stop}) to clear the TL signal before the Tstop temperature value.
5. Rapidly cool the sample back to room temperature.
6. Reheat the sample at the same heating rate (5 K/s), recording the remaining TL curve and noting the position of the first maximum T_m on the TL curve.

Subsequently, repeat the entire process with a slightly lower T_{stop} value (approximately 3 K lower). Fig. 7 illustrates the relationship between T_m and T_{stop}, showing 7 plateaus, each representing a thermoluminescence peak. The peak temperatures T_m for each overlapping peak are as follows: 384, 419, 449, 532, 581, 610, and 640 K. Within the temperature range of 449 K, the peak temperatures of the three overlapping peaks vary with T_{stop}, indicating the significance of their trap recapture electrons process, which aligns with second-order kinetic behavior. After 532 K, the peak temperatures of the remaining 4 overlapping peaks remain relatively constant with T_{stop}, suggesting that the trap recapture electrons process can be neglected, consistent with general or first-order kinetic behavior.

E. Computerized glow curve deconvolution (CGCD)

CGCD method is widely used to study the complex TL mechanism. The position, shape and dynamic parameters of the overlapping peaks in the TL curve can be obtained by using CGCD[44]. Combined with the results of three-dimensional thermoluminescence spectroscopy and T_m-T_{stop} method, CGCD method was used to fit the TL curve of $Y_{1.98}Sm_{0.02}MgTiO_6$ sample irradiated by $^{90}Sr\beta$ radiation source for 100 Gy, and each overlapping peak can be expressed by Formula 1[45] :

$$I(t) = sn_0\exp(-\frac{E}{kT})\cdot[1+\frac{s(b-1)}{\beta}\cdot\int_{T_0}^{T}\exp(-\frac{E}{kT'})dT']^{-\frac{b}{b-1}} \quad (1)$$

In Formula 1: n_0 is the initial number of captured electrons in the trap level; E is the activation energy of the captured electrons, in eV; s is the frequency factor, in Hz; k is the Boltzmann constant, which is 0.862×10^{-4} eV/K; β is the heating rate of the sample, in K/s, which is 5 K/s in this experiment; T is the absolute temperature (in units of K); b is the kinetic order. The result of CGCD fitting is shown in Fig. 8, which can be seen that the fitting curve is in good agreement with the experimental points, and the parameters after fitting are shown in Table 1. Additionally, the kinetic parameters obtained through CGCD fitting allow for the calculation of the energy level lifetime for each overlapping peak. This parameter is crucial and can be used to estimate the saturation dose for each overlapping peak. Such parameters are of significant importance for subsequent dose-response studies. The energy level lifetime for different overlapping peaks can be determined using the following formula 2[46]:

$$\tau = s^{-1}\cdot e^{(\frac{E}{kT})} \quad (2)$$

In Formula 2: τ represents the energy level lifetime of the overlapping peak; s is the frequency factor for the overlapping peak; E denotes the trap depth of the overlapping peak; k is the Boltzmann constant; T stands for the ambient temperature (typically 300 K). After performing the calculations, the results are summarized in Table 1. Notably, the energy level lifetime of the low-temperature overlapping peak at 378 K is relatively short, measuring only 980 seconds. In contrast, the energy level lifetime increases for deeper traps. This behavior arises because electrons captured by traps in the low-temperature peak are more readily released.

In Fig. 8, it can be observed that after CGCD fitting, the peak temperatures of the seven overlapping peaks are as follows: 378 K, 415 K, 477 K, 534 K, 578 K, 615 K, and 654 K. Correspondingly, the trap depths extend from 0.69 eV to 1.49 eV. The b-values for the three overlapping peaks at 378 K, 415 K, and 477 K are 2.0, while the overlapping peak at 534 K has a b-value of 1.6. The three overlapping peaks at 578 K, 615 K, and 654 K have b-values of 1.2, 1.2, and 1.0, respectively, which closely align with the results obtained from the T_m-T_{stop} method. Furthermore, the fitted peak temperatures for the overlapping peaks at 477 K, 534 K, 578 K, 615 K, and 654 K closely match the image in Fig. 5c. Specifically, the three overlapping peaks at 477 K, 534 K, and 578 K are attributed to the Y_2MgTiO_6 matrix, while the overlapping peaks at 615 K and 654 K are associated with Sm^{3+}. However, the overlapping peaks at 378 K and 415 K were not observed in Fig. 5c, possibly due to experimental errors arising from different excitation sources. These results show that on the basis of exploring the internal mechanism of the system, the

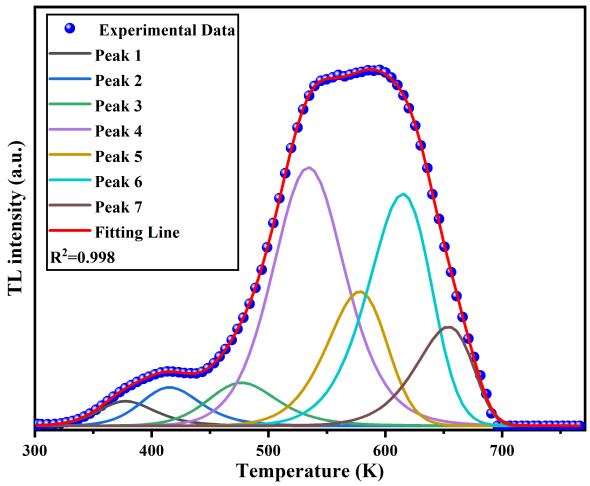

Fig. 8. The TL curve fitting of $Y_{1.98}Sm_{0.02}MgTiO_6$ phosphor by irradiate with $^{90}Sr\beta$ radiation source for 100 Gy was carried out by CGCD method

Table 1. The kinetic parameters of $Y_{1.98}Sm_{0.02}MgTiO_6$ phosphor were analyzed by CGCD method

peaks	E(eV)	T_m(K)	b	s(s^{-1})	τ(s)
1	0.69	378	2.0	$3.95*10^8$	$9.8*10^2$
2	0.81	415	2.0	$1.52*10^9$	$2.6*10^4$
3	0.91	477	2.0	$9.52*10^8$	$2.0*10^6$
4	1.03	534	1.6	$9.96*10^8$	$2.0*10^8$
5	1.22	578	1.2	$9.29*10^9$	$3.3*10^{10}$
6	1.29	615	1.2	$7.04*10^9$	$6.5*10^{11}$
7	1.49	654	1.0	$5.93*10^{10}$	$1.8*10^{14}$

overlapping peak position and kinetic parameters obtained by CGCD fitting have scientific basis and reliability.

F. Dose response

The TL dose response test of $Y_{1.98}Sm_{0.02}MgTiO_6$ phosphor was carried out as follows: 1) preheat the sample to 773 K and hold for 10 s; 2) after cooling to room temperature; 3)irradiate with $^{90}Sr\beta$ radiation source for 2 Gy; 4) measure TL (heating rate is 5 K/s). Repeat the above steps, change the irradiation dose to 5 Gy, 10 Gy, 20 Gy, 50 Gy, 60 Gy, 70 Gy, 80 Gy, 90 Gy, 100 Gy, 110 Gy, 120 Gy, 150 Gy, 200 Gy, 300 Gy, 400 Gy, 500 Gy, 700 Gy, 800 Gy, 900 Gy, 1000 Gy, 2000 Gy, 5000 Gy, 10000 Gy, 20000 Gy and 25000 Gy, and then measure and record the TL luminescence curve, the results are shown in Fig. 9. It can be seen that with the increase of irradiation dose, the shape of the TL curve of the sample has obvious changes. When the irradiation dose is less than 90 Gy, the peak value around 530 K is stronger, when the irradiation dose is more than 90 Gy, the peak value around 610 K is stronger, which indicates that the characteristic thermoluminescence of Sm^{3+} in $Y_{1.98}Sm_{0.02}MgTiO_6$ system is far more sensitive to the irradiation dose than that of Y_2MgTiO_6 matrix. Fig. 10 shows the change of integral intensity of TL

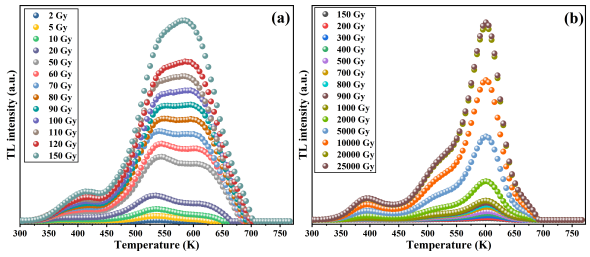

Fig. 9. The thermoluminescence curves of $Y_{1.98}Sm_{0.02}MgTiO_6$ samples by irradiate with $^{90}Sr\beta$ radiation source for different doses

curve at different doses, each experimental point in the figure is the integral area under the TL curve. The dose response may have reached saturation, which can be fitted according to Formula 3[47]:

$$I(D) = A \cdot \left[1 - exp(-\frac{D}{D_0})\right] \tag{3}$$

In Formula 3: I represents the thermoluminescence integral intensity; A denotes the number of thermoluminescent sensitive units in the measured sample; D stands for the radiation dose; D_0 corresponds to the saturation dose. After fitting, it was found that the saturation dose of the sample was 9956 Gy, Compared with the commonly used thermoluminescence dosimeter (such as LiF:(Mg,Cu,P),BeO,Al_2O_3:C), this material has a higher saturation dose, and the dose response can still maintain good linearity at 1 kGy. Because the electrons trapped by the low temperature peak trap are more easily released, the decay time of the trapped electrons at 378 K is only 0.01 days, and the decay time of the trapped electrons at 415 K is 0.3 days. However, the decay time of the trapped reactivated electrons at 477 K and after is more than 23 days, indicating that the decay time of the material is longer. Therefore, this material can be used as a thermoluminescence dosimeter for high-dose occasions, such as in the field of fruit radiation preservation.

For a TL curve composed of multiple overlapping peaks, it is indeed possible to fit the dose response using the total integral of TL curves obtained at different irradiation doses. Due to significant differences in the energy level lifetimes of each overlapping peak, there are some deviations in theory. Nevertheless, within specific dose ranges, these deviations are not pronounced. To explore the dose response characteristics of each overlapping peak in the $Y_{1.98}Sm_{0.02}MgTiO_6$ phosphor system, the CGCD method was employed to fit TL curves at various irradiation doses, followed by further analysis. The results are depicted in Fig. 11. In Fig. 11, it can be observed that the peak temperatures T_m of Peaks 1, 2, and 3 shift toward lower temperatures as the irradiation dose increases, consistent with second-order kinetic behavior. Peaks 4, 5, 6, and 7, on the other hand, exhibit no significant change in T_m with increasing irradiation dose, aligning with first-order kinetic behavior and the results are consistent with those of T_m-T_{stop} method.

With the increase of irradiation dose, the thermoluminescence intensity of peak 1 did not increase significantly after

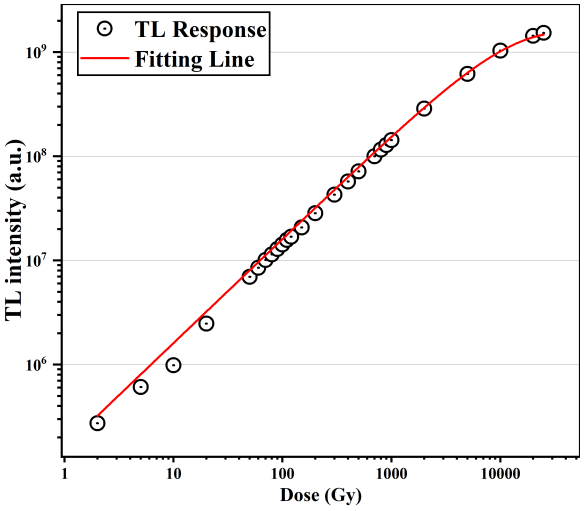

Fig. 10. Dose response curve of $Y_{1.98}Sm_{0.02}MgTiO_6$ sample

200 Gy. In order to explore the dose response curve of different overlapping peaks, the thermoluminescence integral intensity of each overlapping peak under different irradiation doses was made according to Fig. 11. The results are shown in Fig. 12. It can be seen that except for peak 1, the other overlapping peaks are in good agreement with the linear relationship, and the slopes of peak 6 and peak 7 are similar, and the slopes of peaks 3, 4 and 5 are consistent, which indicates that peaks 6 and 7 may be caused by Sm^{3+}, peaks 3, 4 and 5 are caused by the matrix, and the slope of peak 6 is significantly larger than that of peak 4, indicating that the characteristic thermoluminescence of Sm^{3+} is much more sensitive to the irradiation dose than the matrix. The dose response of peak 1 may have reached saturation. After fitting using Formula 3, the saturation dose for Peak 1 is determined to be 102.5 ± 3.2 Gy. Considering that the dose rate of the $^{90}Sr\beta$ radioactive source is 0.1 Gy/s, and the energy level lifetime of Peak 1 is 980 seconds, it is estimated that Peak 1 reaches saturation at an irradiation dose of approximately 98 Gy. Experimental dose-response measurements for Peak 1 confirm this hypothesis. To enhance the saturation dose for Peak 1, one could choose a radiation source with a higher dose rate. In an ideal scenario, for precise measurements of doses below KGy, eliminating Peak 1 and utilizing TL integration after 378 K would be suitable. For measurements of doses above KGy, eliminating both Peak 1 and Peak 2 (with a saturation dose of approximately 2.6 KGy) and using TL integration after 415 K would be appropriate.

G. Repeatability test

To verify the repeatability of the thermoluminescence (TL) signal, the TL curves of $Y_{1.98}Sm_{0.02}MgTiO_6$ phosphor were measured multiple times under 100 Gy irradiation. Fig. 13 shows the results of 12 measurements, where the total integral of the TL curve from each measurement was selected as

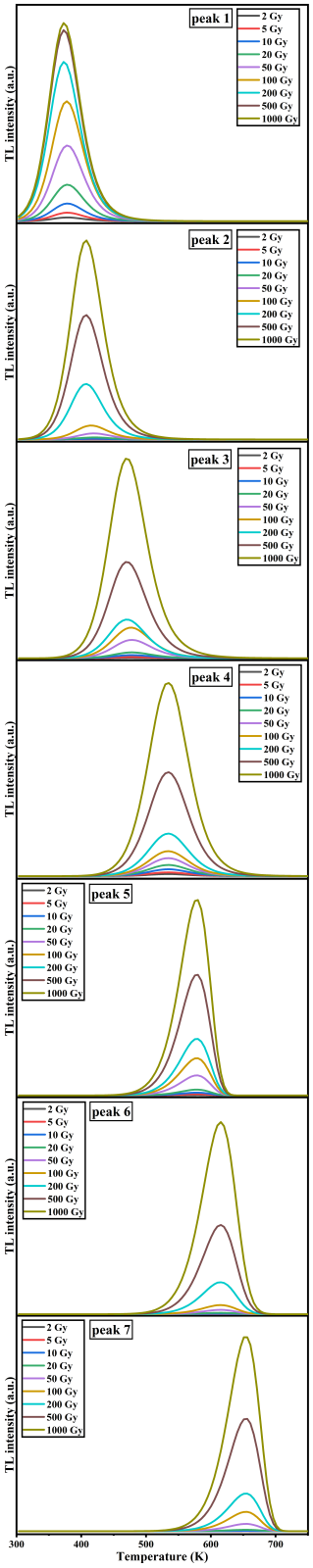

Fig. 11. Overlapping peak curves at different irradiation doses

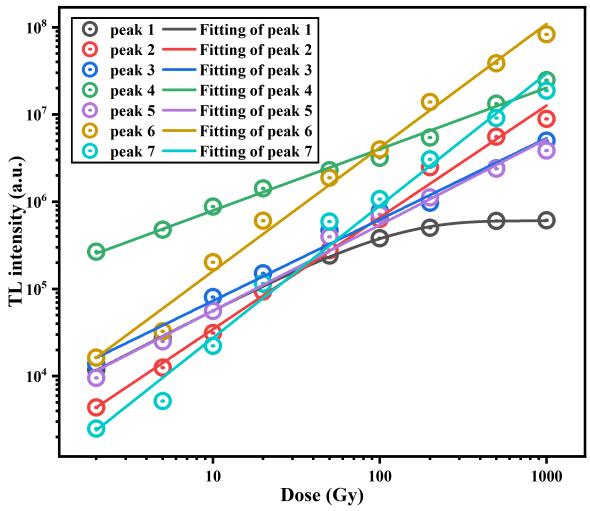

Fig. 12. Dose response curves of different overlapping peak

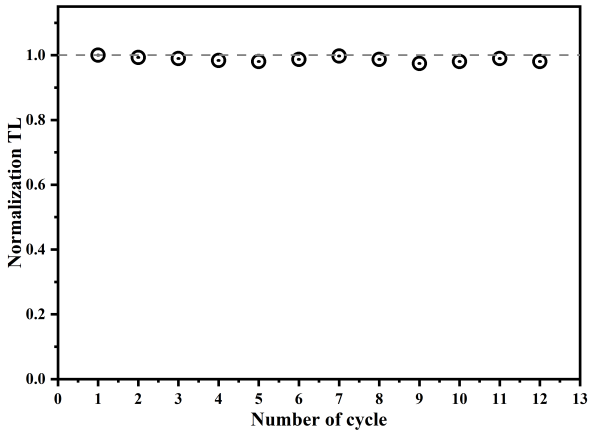

Fig. 13. Repetitive experiment of thermoluminescence

the outcome and normalized. The experimental results indicate a relative standard error of approximately 0.06% for the measured TL signal. Therefore, TL measurements are minimally affected by radiation and temperature

IV. CONCLUSION

$Y_{2-x}Sm_xMgTiO_6$ ($0 \leq x \leq 0.2$) series phosphors were prepared by high-temperature solid-state method, and XRD proved that Sm^{3+} successfully entered the lattice and replaced Y^{3+}. PL proved that there were four emission peaks at 568 nm, 605 nm, 652 nm and 715 nm under 409 nm excitation. By analyzing the TL curve of the sample, it was found that the TL of $Y_{1.98}Sm_{0.02}MgTiO_6$ sample was the strongest, and three-dimensional thermoluminescence spectrum showed that the thermoluminescence around 530 K was attributed to Y_2MgTiO_6 matrix, and the thermoluminescence around 610 K was related to Sm^{3+} defects, which also proved that the matrix was less affected by concentration quenching than Sm^{3+}. The T_m-T_{stop} method indicates that the thermoluminescence (TL) spectrum of this phosphor is a superposition of seven peaks. The Tm values for each overlapping peak are as follows: 384, 419, 449, 532, 581, 610, and 640 K. Additionally, the kinetic order for each peak can be roughly estimated. Utilizing information from the three-dimensional thermoluminescence spectrum and the T_m-T_{stop} method, the TL curve of the sample was fitted using the CGCD method, yielding reliable results. The trap parameters corresponding to the seven overlapping peaks are as follows: 0.69, 0.81, 0.91, 1.03, 1.22, 1.29, and 1.49 eV, with energy level lifetimes of $9.8*10^2$, $2.6*10^4$, $2.0*10^6$, $2.0*10^8$, $3.3*10^{10}$, $6.5*10^{11}$, $1.8*10^{14}$, respectively. The saturation dose of $Y_{1.98}Sm_{0.02}MgTiO_6$ sample is higher, at 9956 Gy. Notably, this phosphor demonstrates good thermal stability and low production cost, making it suitable for thermoluminescence dosimetry applications in high-dose radiation monitoring. To ensure accurate dose monitoring, dose-response curves were generated for each overlapping peak. Within the 1 kGy range, Peak 1 has already reached saturation (at 102 Gy), while the other peaks exhibit linear behavior. For precise measurements of doses below kGy, TL integration after 378 K is recommended. For more accurate measurements of doses above kGy, TL integration after 415 K is preferable.

[1] Y. Wang, H. Chen, F. Chen, et al., Radiation dose detection using a high-power portable optically stimulated luminescence real-time reading system. Nucl. Sci. Tech. 29 (10), 63-71 (2018). doi: 10.1007/s41365-018-0484-z.

[2] Z.W. Lv, G.X. Wei, H.Q. Wang, et al., New flexible $CsPbBr_3$-based scintillator for X-ray tomography. Nucl. Sci. Tech. 33 (08), 36-46 (2022). doi: 10.1007/s41365-022-01085-z.

[3] Y. Chuan, L.D.G Xu, P.C. Zhang, Preparation and characterization of Bi_2O_3/XNBR flexible films for attenuating gamma rays. Nucl. Sci. Tech. 29 (07), 28-39 (2018). doi: 10.1007/s41365-018-0436-7.

[4] S.L. Jin, R.F. Li, H. Huang, Compact ultrabroadband light-emitting diodes based on lanthanide-doped lead-free double perovskites. Light Sci. Appl. 11, 52 (2022). doi: 10.1038/s41377-022-00739-2.

[5] X.B. Li, Q. Liu, W.T. Huang, Structural and luminescent properties of Eu^{3+}-doped double perovskite $BaLaMgNbO_6$ phosphor. Ceram. Int. 44(2), 1909–1915 (2018). doi: 10.1016/j.ceramint.2017.10.130.

[6] C.Z. Guan, J. Zhou, H.L. Bao, et al., Study of the relationship between the local geometric structure and the stability of $La_{0.6}Sr_{0.4}MnO_{3-\delta}$ and $La_{0.6}Sr_{0.4}FeO_{3-\delta}$ electrodes. Nucl. Sci. Tech. 30(02), 98-105 (2019). doi: 10.1007/s41365-019-0550-1.

[7] Z.M. Chen, Z.Y. Wang, W.D. Kang, Preparation and luminescent properties of double perovskite-type $La_{2-x-y}Y_xMgTiO_6$:yEu^{3+} red fluorescent materials. J. Lumin. 243, 118656 (2022). doi: 10.1016/j.jlumin.2021.118656.

[8] T. Zheng, L.H. Luo, P. Du, Highly-efficient double perovskite Mn^{4+}-activated Gd_2ZnTiO_6 phosphors: a bifunctional optical sensing platform for luminescence thermometry and manometry. Chem. Eng. J. 446, 136839 (2022). doi: 10.1016/j.cej.2022.136839.

[9] D.J. Hou, S.M. Zheng, Z.S. Lin, et al., A Mn^{4+} activated $(Gd,La)_2(Zn,Mg)TiO_6$ deep-red emission phosphor: The luminescence properties and potential application for full-spectrum pc-LEDs. J. Lumin. 247, 118895 (2022). doi: 10.1016/j.jlumin.2022.118895.

[10] J.Q. Li, J.S. Liao, H.R. Wen, Multiwavelength near infrared downshift and downconversion emission of Tm^{3+} in double perovskite Y_2MgTiO_6:Mn^{4+}/Tm^{3+} phosphors via resonance energy transfer. J. Lumin. 213, 356–363 (2019). doi: 10.1016/j.jlumin.2019.05.038.

[11] J. Xu, S. Tanabe, Persistent luminescence instead of phosphorescence:history, mechanism, and perspective. J. Lumin. 205, 581–620 (2019). doi: 10.1016/j.jlumin.2018.09.047.

[12] H.H. Xiao, L.L. Liu, W.Y. Li, et al., TLD calibration and absorbed dose measurement in a radiation-induced liver injury model under a linear accelerator. Nucl. Sci. Tech. 34, 53 (2023). doi: 10.1007/s41365-023-01211-5.

[13] X.M. Jin, Y. Liu, C.L. Su, et al., Ionizing and non-ionizing kerma factors in silicon for China Spallation Neutron Source neutron spectrum. Nucl. Sci. Tech. 30, 143 (2019). doi: 10.1007/s41365-019-0664-5.

[14] Y.L. Liu, Q.X. Zhang, J. Zhang, et al., Quantitative energy-dispersive X-ray fluorescence analysis for unknown samples using full-spectrum least-squares regression. Nucl. Sci. Tech. 30, 52 (2019). doi: 10.1007/s41365-019-0564-8.

[15] Y.H, Wang, Q. Li, L. Chen, et al., Simulation study of the dose and energy responses of FNTD personal neutron dosimetry. Nucl. Sci. Tech. 30, 32 (2019). doi: 10.1007/s41365-019-0546-x.

[16] H. Yang, X.Y. Zhang, W.G. Gu, et al., A novel method for gamma spectrum analysis of low-level and intermediate-level radioactive waste. Nucl. Sci. Tech. 34, 87 (2023). doi: 10.1007/s41365-023-01236-w.

[17] K.N. Li, X.P. Zhang, Q. Gui, et al., Characterization of the new scintillator Cs_2LiYCl_6:Ce^{3+}. Nucl. Sci. Tech. 29, 11 (2018). doi: 10.1007/s41365-017-0342-4.

[18] W. Tang, C.D. Zuo, Y.K. Li, Exploiting intervalence charge-transfer engineering to finely control $(Ba,Sr)TiO_3$:Pr^{3+} luminescence thermometers. J. Lumin. 236, 118103 (2021). doi: 10.1016/j.jlumin.2021.118103.

[19] Cheng-lin. G, Dubey. V, Kushwah. K.K., et al., Thermoluminescence Studies of β and γ-Irradiated Geological Materials for Environment Monitoring. J. Fluoresc. 30, 819–825 (2020). doi: 10.1007/s10895-020-02536-9.

[20] S.Y. Zhang, K.Y. Tang, H.J. Fan, et al., A competitive radioluminescence material - LiF:Mg,Cu,P for real-time dosimetry. Radiat. 151, 106719 (2022). doi: 10.1016/j.radmeas.2022.106719.

[21] Z.Y. Xiong, Q. Tang, C.X. Zhang, Investigation of thermoluminescence in $Li_2B_4O_7$ phosphors doped with Cu, Ag and Mg. Sci. China. Ser. G. 50, 311–320 (2007). doi: 10.1007/s11433-007-0020-3.

[22] H.Y. Xiao, G. Duan, X.T. Zu, et al., Ab initio molecular dynamics simulation of pressure-induced phase transformation in BeO. J. Mater. Sci. 46, 6408–6415 (2011). doi: 10.1007/s10853-011-5590-9.

[23] Y. Wang, N. Can, P.D. Townsend, Influence of Li dopants on thermoluminescence spectra of $CaSO_4$ doped with Dy or Tm. J. Lumin. 131(9), 1864-1868 (2011). doi: 10.1016/j.jlumin.2011.04.042.

[24] Pietriková. M, Krása. J, Juha. L, Thermoluminescence glow curves of CaF_2: Dy crystals irradiated by soft X-rays. Z. Physik B - Condensed Matter. 93, 63–66 (1993). doi: 10.1007/BF01308808.

[25] Y.W. Wei, Y.J. Dong, T. Zhang, et al., Influence of reaction of Al_2O_3 and carbonaceous materials in Al_2O_3–C refractories on aluminum and carbon pick-up of iron. J. Iron Steel Res. Int. 27, 55–61 (2020). doi: 10.1007/s42243-019-00352-5.

[26] W.J. Ma, Q. Tang, C.X. Zhang, et al., Thermoluminescent spectra of MgB_4O_7 doped with Mn and Dy. Nuclear Techniques. 33(01), 31-34 (2010).(chinese)

[27] Gavhane K.H., Bhadane M.S., Kulkarni P.P., Investigation of novel Eu doped $SrDy_2O_4$ microphosphor for thermoluminescence dosimetry. J. Lumin. 231, 117781 (2021). doi: 10.1016/j.jlumin.2020.117781.

[28] Kishor H. Gavhane, Mahesh S. Bhadane, Preeti P. Kulkarni, et al., Investigation of novel Eu doped $SrDy_2O_4$ microphosphor for thermoluminescence dosimetry. J. Lumin. 231, 117781 (2021). doi: 10.1016/j.jlumin.2020.117781.

[29] Alajlani Y, Can N, Thermoluminescence glow curve analysis and kinetic parameters of Dy-doped $BaSi_2O_5$ phosphor. J. Rare Earths. 40 (2), 234–242 (2022). doi: 10.1016/j.jre.2020.10.020.

[30] I.C. Chen, T.M. Chen, Sol-gel synthesis and the effect of boron addition on the phosphorescent properties of $SrAl_2O_4$:Eu^{2+},Dy^{3+} phosphors. J. Mater. 16, 644–651 (2001). doi: 10.1557/JMR.2001.0122.

[31] Chernov V, Salas-Castillo P, Díaz-Torres L A, Thermoluminescence and infrared stimulated luminescence in long persistent monoclinic $SrAl_2O_4$:Eu^{2+},Dy^{3+} and $SrAl_2O_4$:Eu^{2+}, Nd^{3+} phosphors. Opt. Mater. 92, 46–52 (2019). doi: 10.1016/j.optmat.2019.04.015.

[32] Som S, Chowdhury M, Sharma S K, Kinetic parameters of γ-irradiated Y_2O_3 phosphors: effect of doping/codoping and heating rate. Radiat. Phys. Chem. 110, 51–58 (2015). doi: 10.1016/j.radphyschem.2015. 01.015.

[33] B. Zhao, S.L. Hu, D. Wang, Inhibitory effect of gamma irradiation on Penicillium digitatum and its application in the preservation of Ponkan fruit. Sci. Hortic. 272, 109598 (2020). doi: 10.1016/j.scienta. 2020.109598.

[34] F.M. Li, Y.B. Gu, D.H. Chen, Study on radiation preservation of frozen egg liquid. Radiat. Phys. Chem. 57 (3–6), 341–343 (2000). doi: 10.1016/S0969-806X(99)00401-6.

[35] Shannon R.D.J., Revised Effective Ionic Radii and Systematic Study of Inter Atomic Distances in Halides and Chalcogenides. Acta. Crystallogr. A. 32 (SEP1), 751-767 (1976). doi: 10.1107/S0567739476001551.

[36] H. Yang, S. Zhang, H. Yang, et al., Vibrational spectroscopic and crystal chemical analyses of double perovskite Y2MgTiO6 microwave dielectric ceramics. J. Am. Ceram. 103, 16737 (2019). doi: 10.1111/jace.16737.

[37] H. Liu, J.Y. Guo, X.Y. Li, et al., Luminescence and temperature sensing properties of $Y_{2-x-y}Tm_xSm_yMgTiO_6$ phosphors. J. Lumin. 267, 120392 (2024). doi: 10.1016/j.jlumin.2023.120392.

[38] Z.T. Fan, S.L. Bi, J. Wang, et al., Photoluminescence properties and energy transfer of double perovskite Ca_2LaTaO_6:Bi^{3+},Tb^{3+} phosphor. J. Lumin. 252, 119396 (2022). doi: 10.1016/j.jlumin.2022.119396.

[39] K. Li, D. Mara, Van Deun R, Synthesis and luminescence properties of a novel dazzling red-emitting phosphor $NaSr_3SbO_6$:Mn^{4+} for UV/n-UV w-LEDs. Dalton Trans.

(2019). doi: 10.1039/C8DT04827D.
[40] H. Liu, J.Y. Guo, J.Y. Xu, et al., Luminescence properties and energy-transfer behavior of $Y_{2-x-y}Bi_xEu_yMgTiO_6$ phosphors. Heliyon. 9 (8), e19063 (2023). doi: 10.1016/j.heliyon.2023.e19063.
[41] T. Srikanth, D.V. Krishna Reddy, K.S. Rudramamba, et al., Red light component tuning by n-UV/blue light excitations in Sm^{3+}/Eu^{3+} co-doped Y_2O_3–Al_2O_3–Bi_2O_3–B_2O_3–SiO_2 glasses for W-LED applications. Opt. Mater. 134, 113148 (2022). doi: 10.1016/j.optmat.2022.113148.
[42] N.S. Huang, K. Li, H.X. Deng, BRIGHT: the three-dimensional X-ray crystal Bragg diffraction code. Nucl. Sci. Tech. 30, 39 (2019). doi: 10.1007/s41365-019-0559-5.
[43] Yadav R S, Energy transfer induced color tunable photoluminescence in Tb^{3+}/Sm^{3+} co-doped Y_2O_3 nano-phosphor for warm white LEDs. J. Alloys Compd. 931, 167579 (2023). doi: 10.1016/j.jallcom.2022.167579.
[44] H. Liu, Z.Y. Xiong, C.X. Zeng, et al., Luminescence characteristics of $Y_{2-x-y}Bi_xEu_yMgTiO_6$ phosphors. Nuclear Techniques. 46, 060501(2023). doi: 10.11889/j.0253-3219.2023.hjs.46.060501. (chinese)
[45] Z.Y. Xiong, X.C. Wang, Y.T. Liang, et al., Study of thermoluminescence, photoluminescence and dosimetry for the YAGG:Ce($Y_{2.96}Al_{3.4}Ga_{1.6}O_{12}$:0.04Ce) phosphor. Appl. Radiat. Isot. 193, 110615(2023). doi: 10.1016/j.apradiso.2022.110615.
[46] J.Y. Guo, M. Gao, Z.Y. Xiong, et al., Thermoluminescence of Natural Quartz Grains Beside Huguangyan Maar Lake. J. Phys. Conf. Ser. 2470 (1), 012004 (2023). doi: 10.1088/1742-6596/2470/1/012004.
[47] M.L. Zhan, Y.Y. Chen, Z. Xu, et al., Investigation on thermoluminescence of phosphor YGaAG:Ce($Y_{2.96}Ce_{0.04}Al_{3.4}Ga_{1.6}O_{12}$). Nuclear Techniques. 43 (5), 050501 (2020). doi: 10.11889/j.0253-3219.2020.hjs.43.050501. (chinese)